CHEMISTRY OF MATERIALS
Cite This: Chem. Mater. 2017, 29, 10426−10435
Article
pubs.acs.org/cm

Low Thermal Conductivity and High Thermoelectric Performance in Sb and Bi Codoped GeTe: Complementary Effect of Band Convergence and Nanostructuring

Suresh Perumal,[†] Pavithra Bellare,[‡] U. Sandhya Shenoy,[§] Umesh V. Waghmare,[§] and Kanishka Biswas*[,†]

[†]New Chemistry Unit, Jawaharlal Nehru Centre for Advanced Scientific Research (JNCASR), Jakkur P.O., Bangalore 560064, India
[‡]Materials Research Centre, Indian Institute of Science, Bangalore 560 012, India
[§]Theoretical Sciences Unit, Jawaharlal Nehru Centre for Advanced Scientific Research (JNCASR), Jakkur P.O., Bangalore 560064, India

Supporting Information

ABSTRACT: Complementary and beneficial effects of Sb and Bi codoping in GeTe are shown to generate high thermoelectric figure of merit, zT, of 1.8 at 725 K in $Ge_{1-x-y}Bi_xSb_yTe$ samples. Sb and Bi codoping in GeTe facilitates the valence band convergence enhancing the Seebeck coefficient as supported by density functional theoretical (DFT) calculations. Further, Sb and Bi codoping in GeTe releases the rhombohedral strain and increases its tendency to be cubic in structure, which ultimately enhances the valence band degeneracy. At the same time, Bi forms nanoprecipitates of size ∼5−20 nm in GeTe matrix and Sb doping increases solid solution point defects greatly, which altogether scatter low-to mid wavelength phonons and result in reduced lattice thermal conductivity down to 0.5 W/mK in the 300−750 K range.

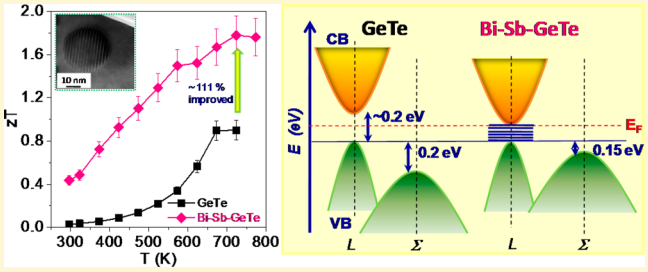

INTRODUCTION

Thermoelectric materials have received great attention recently as they can directly and reversibly convert a significant fraction of waste heat into usable electricity and they are thus expected to play a significant role in future energy utilization and management.[1−4] Thermoelectric conversion efficiency is strongly coupled with a dimensionless figure of merit (zT), which is described as,

$$zT = \frac{S^2\sigma}{\kappa_{total}}T$$

where S, σ, κ_{total}, and T represent Seebeck coefficient, electrical conductivity, total thermal conductivity, and absolute temperature, respectively. In order to achieve high zT in materials, one has to enhance the power factor ($S^2\sigma$) and/or reduce κ_{total} as much as possible. The thermoelectric community has engaged in significant effort to simultaneously enhance the Seebeck coefficient (by minority carrier energy filtering,[5] creation of a resonant states in electronic structure near the Fermi level,[6] convergence of electronics sub-bands,[7,8] and quantum confinement[9]) and reduce the lattice thermal conductivity, κ_{lat} (by phonon scattering due to nano/mesoscale precipitates, grain boundaries;[10,11] and intrinsic bond anharmonicity[12,13]).

Among IV−VI semiconductors, PbTe based n- and p-type materials have been extensively studied for midtemperature (600−900 K) thermoelectric application,[6,7,10,11] whereas GeTe and SnTe based compounds were somewhat ignored due to their high p-type carrier density, n_p, (∼10^{20}−10^{21} cm^{-3}) caused by intrinsically high cation (Ge/Sn) vacancies and resulting in rather low S with high κ_{el} (electronic thermal conductivity).[14−17] However, the toxic nature of Pb puts a limitation on practical applications and necessitates the search for alternative Pb-free thermoelectric materials. GeTe and SnTe based systems have been recently relooked at and proposed to be promising thermoelectric materials after tailoring their properties with suitable dopants and introduction of band convergence and nanostructuring.[17−19] In GeTe, many strategies have been adopted with the aim to either enhance the power factor, $S^2\sigma$, or to reduce the κ_{lat} in compositions such as $Ge_{1-x}Pb_xTe$,[20,21] GeTe-$AgSbTe_2$ (TAGS-x),[22−24] GeTe-$AgSbSe_2$ (TAGSSe-x),[25] $Sb_2Te_3(GeTe)_n$ (GST),[26] and Sb/Bisingle doped GeTe,[27,28] $GeTe_{1-x}Se_x$,[29] and GeTe-GeSe-GeS.[30]

Pristine GeTe crystallizes in rhombohedral α-GeTe (space group $R3m$) structure at room temperature and rocksalt β-GeTe (space group Fm-$3m$) at high temperature. GeTe undergoes a ferroelectric structural transition of $R3m \rightarrow Fm$-$3m$ in the temperature range of 673−703 K[30] (see Figure 1) involving a strain and slight displacement of Ge atoms from (1/

Received: September 22, 2017
Revised: November 29, 2017
Published: November 29, 2017

DOI: 10.1021/acs.chemmater.7b04023
Chem. Mater. 2017, 29, 10426−10435

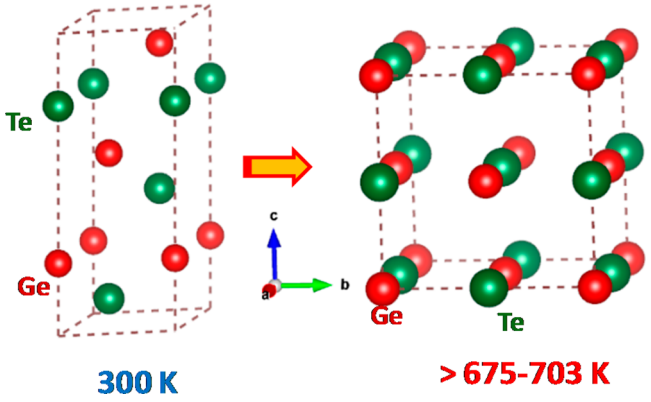

Figure 1. Crystal structure of GeTe represents the ferroelectric structural transition ($R3m \rightarrow Fm\text{-}3m$). At 300 K, GeTe possesses a rhombohedral structure ($R3m$) which transforms to cubic ($Fm\text{-}3m$) above 675 K.

2, 1/2, 1/2) to (1/2-x, 1/2-x, 1/2-x) in the low T phase. It gives a polarization along the body cell diagonal and subsequent shear distortion along the [111] direction, making the angular distortion of $\alpha = 1.65°$.[19,31−33] In terms of thermoelectric properties, pristine GeTe possesses σ, S, and κ_{total} values of ~8500 S/cm, ~30 μV/K, and ~8 W/mK at 300 K, respectively, which results in a reasonable thermoelectric figure of merit, zT , of ~0.8 at 720 K.[34]

Recently, we have shown that 10 mol % of Sb doping in GeTe yields a significantly high Seebeck coefficient.[27] However, the concrete reason behind the high Seebeck coefficient obtained upon Sb doping in GeTe has not yet been understood. Further, 6 mol % of Bi alloying in GeTe has shown to have an extremely low lattice thermal conductivity (κ_{lat}) due to increased scattering of low-to-mid wavelength heat carrying phonons by nanostructuring.[28] Here, with an aim to understand the physical significance of the enhanced Seebeck coefficient upon Sb doping in GeTe and to introduce the low thermal conductivity in the Sb doped GeTe system, we take up the codoping of Bi and Sb in GeTe and investigate their structural, optical, electronic, and thermoelectric properties. As Sb and Bi have distinct but complementary roles, we expect codoping of Sb and Bi in GeTe to result in a synergistic effect of enhancement of Seebeck coefficient and reduction of thermal conductivity.

Herein, we report the impurity defect states induced high thermoelectric performance in $Ge_{1-x-y}Bi_xSb_yTe$ (x = 0.02, 0.05; y = 0.05, 0.1) synthesized by sealed tube melting followed by hot-pressing. Codoping of Sb and Bi in GeTe eliminates intrinsic Ge vacancies and thereby reduces the excess p-type carrier concentration (n_p) in GeTe. Importantly, Sb and Bi codoping enhances the Seebeck coefficient significantly in $Ge_{1-x-y}Bi_xSb_yTe$. The reason behind the high Seebeck coefficient is clearly examined by density functional theory (DFT) calculations of the electronic structure, showing that codoping of Sb and Bi closes the principal band gap by introducing donor Bi or Sb energy levels just below the conduction band and also triggers the electronic subvalence band conduction by reducing the energy separation between light and heavy hole valence bands of GeTe. Further, the codoping of Sb and Bi in GeTe suppresses the κ_{lat} to an ultralow value of ~0.5 W/mK due to scattering of heat carrying phonons by nanoprecipitates formed of Bi and excess point defects by Sb substitution. Thus, a maximum thermoelectric figure of merit (zT_{max}) of ~1.8 at ~725 K is achieved at the composition of $Ge_{1-x-y}Bi_xSb_yTe$ (x = 0.05; y = 0.1), which is ~111% higher than that of pure GeTe.

EXPERIMENTAL SECTION

Synthesis. High quality ingots with about ~6 g scale of $Ge_{1-x}Sb_xTe$ (x = 0−0.15), $Ge_{1-x}Bi_xTe$ (x = 0−0.15), and $Ge_{1-x-y}Bi_xSb_yTe$ (x = 0.02, 0.05; y = 0.05, 0.1) were synthesized by vacuum sealed tube reaction. Typically, appropriate ratios of high purity starting materials of Ge, Sb, Bi, and Te were taken in a quartz tube and sealed under a vacuum pressure of 10^{-6} Torr. The sealed tubes were slowly heated to 1223 K over 10 h, then soaked for 6 h, and slowly cooled to room temperature over 10 h using a programmable furnace.

In order to obtain the highly dense pellets for the thermoelectric measurements, the crushed fine powders were hot-pressed at ~873 K with the pressure of about 45 MPa for the duration of 7 min under argon atmosphere using a induction hot uniaxial pressing.[35] The density, ρ, of all of the compacted pellets was measured by Archimedes method, and the densities of the measured samples were around ~97% of theoretical density.

Characterizations. All of the samples obtained by the above processes were crushed into fine powers for structural analysis using Powder X-ray diffraction (PXRD), which has been recorded using Cu Kα (λ = 1.5406 Å) radiation on a Bruker D8 diffractometer. TEM micrographs were acquired using a FEI Tecnai T20 instrument operated at an accelerating voltage of 200 kV.

The room temperature optical band gaps of all of the samples were estimated by the diffuse reflectance measurement using a FT-IR Bruker IFS 66 V/S spectrometer in the wavenumber range 4000−400 cm^{-1} with 2 cm^{-1} resolution and 50 scans. Absorption (α/Λ) data were calculated from reflectance data using the Kubelka−Munk equation: $\alpha/\Lambda = (1 - R)^2/(2R)$, where R is the reflectance and α and Λ are the absorption and scattering coefficient, respectively. The energy band gaps were derived from an α/Λ vs E_g (eV) plot. In order to probe the rhombohedral to cube transition temperature, differential scanning calorimetry (DSC) was carried out with a heating rate of 5 K/min for the samples of $Ge_{1-x-y}Bi_xSb_yTe$ using DSC Q2000 TA Instruments.

Thermoelectric Measurements. The electronic properties such as electrical conductivity and Seebeck coefficients were simultaneously measured under He atmosphere from room temperature to 773 K by a ULVAC-RIKO ZEM-3 instrument. The sample dimensions of ~2 × 2 × 8 mm^3 were used for all measurements. THe Hall measurement was carried out at room temperature in a homemade setup, where the variable magnetic field and dc current used were 0−0.5 T and 50 mA, respectively. The carrier concentration of holes (n_p) was calculated from the equations of $n_p = 1/(eR_H)$, where R_H is the Hall coefficient and e is an electronic charge. The Hall carrier motility, μ_H, of all samples was estimated using the expression $\mu_H = R_H\sigma$. Thermal diffusivity, D, was directly measured in the range 300−773 K by using the laser flash diffusivity method in a Netzsch LFA-457. Coins with ~8 mm diameter and ~2 mm thickness were used in all of the measurements. Temperature dependent heat capacity, C_p, was derived using standard pyroceram in LFA-457, which is in good agreement with the Dulong−Petit C_p value. The total thermal conductivity, κ_{total}, was calculated using the formula $\kappa_{total} = DC_p\rho$, where ρ is the density. Electrical and thermal transport measurements were performed in a similar direction.

Computational Details. The electronic structure of GeTe, Bi-doped, Sb-doped, and Bi−Sb codoped GeTe were determined within first-principles density functional theory (DFT) using the Quantum Espresso package.[36] Valence and semicore electronic states of Ge, Te, Bi, and Sb (in $3d^{10}$ $4s^2$ $4p^2$, $4d^{10}$ $5s^2$ $5p^4$, $5d^{10}$ $6s^2$ $6p^3$, and $4d^{10}$ $5s^2$ $5p^3$ configurations, respectively) were treated through the use of pseudopotentials. Fully relativistic (to include the effect of spin orbit coupling) ultrasoft pseudopotentials and a generalized gradient approximation (GGA) to exchange-correlation energy with parametrized functional of Perdew, Burke, and Erzenhoff (PBE) were used.[37] Pristine, singly doped, and codoped samples were simulated

DOI: 10.1021/acs.chemmater.7b04023
Chem. Mater. 2017, 29, 10426−10435

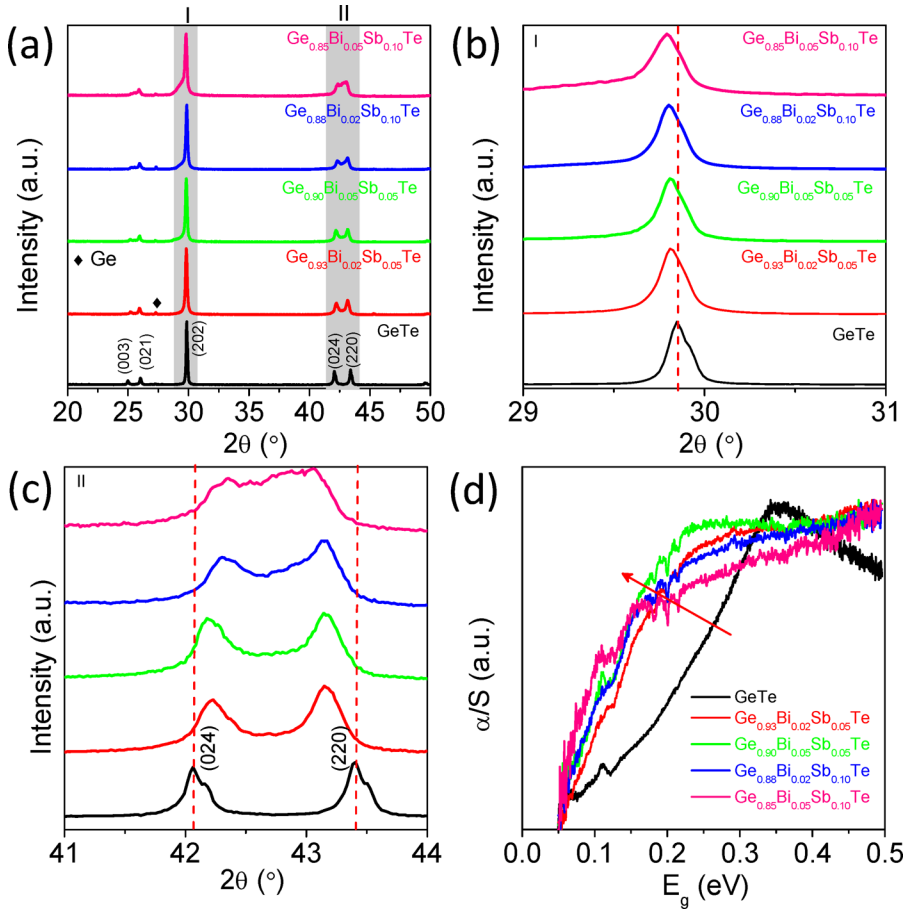

Figure 2. (a) PXRD patterns of $Ge_{1-x-y}Bi_xSb_yTe$ (x = 0.02, 0.05; y = 0.05, 0.1), (b) enlarged version of PXRD shows shift in the high intensity peak (202), and (c) enlarged version of PXRD in the angels (2θ) between 41 and 44°. (d) Electronic absorption spectra of Bi and Sb codoped GeTe.

with a tetragonal supercell ($\sqrt{2} \times \sqrt{2} \times 2$) containing 32 atoms. In distorted cubic GeTe ($R3m$), splitting of initially degenerate bands are negligible, thus GeTe is treated in an ordered-cubic ($Fm\bar{3}m$) structure here similar to earlier calculations.[21] Plane wave basis for representing Kohn–Sham wave functions was terminated with an energy cutoff of 40 Ry and that for charge density with a cutoff of 320 Ry. 8 × 8 × 6 meshes of k points were used in sampling the Brillouin zone (of the supercell) integrations. The discontinuity in occupation numbers of electronic states was smoothed using the Fermi–Dirac distribution function with a smearing width (k_BT) of 0.04 eV. Electronic structures were determined along high symmetry lines (Γ - X - M - Γ - Z - R - A - Z) in the Brillouin zone.

RESULTS AND DISCUSSION

Figure 2 presents the powder X-ray diffraction (PXRD) patterns of $Ge_{1-x-y}Bi_xSb_yTe$ (x = 0.02, 0.05; y = 0.05, 0.1) and all of the patterns could be indexed with a rhombohedral GeTe structure (space group $R3m$). However, a small fraction of Ge peaks was generally seen in all samples due to intrinsic Ge vacancies, thereby GeTe always prefers to be in Te-rich composition, which agrees with previous experiments.[19,27,28,34,38] Figure 2a shows the PXRD pattern of $Ge_{1-x-y}Bi_xSb_yTe$ (x = 0.02, 0.05; y = 0.05, 0.1) samples, and the high intensity peak at 2θ of 29.88° is further enlarged and presented in Figure 2b. The shift in the high intensity peak toward lower 2θ angle side upon simultaneous codoping of Sb and Bi in GeTe indicates the solid solubility of Sb and Bi in GeTe within the detection limit of XRD. This shift is associated with the substitution of the larger atomic radius of Bi (1.43 Å) and Sb (1.33 Å) in place of smaller Ge (1.25 Å) in GeTe. The calculated lattice constants are $a = b$ = 4.1664(2) Å and c = 10.6707(4) Å and $a = b$ = 4.1847 (2) Å and c = 10.4547 (3) Å, for GeTe and $Ge_{0.85}Bi_{0.05}Sb_{0.10}Te$, respectively, which indicate that lattice parameters a and b increase with the addition of Bi and Sb in GeTe, while the lattice parameter c contracts. In pristine GeTe, the presence of double-peaks [(024) and (220)] in between 2θ of 41–45° indicates a rhombohedral structure (see Figure 2c) at room temperature. These double peaks get closer and try to merge when the concentration of Sb and Bi increases in GeTe, which suggests that the Sb and Bi codoping relaxes the rhombohedral structure due to their larger atomic radii as compared to Ge, thus pushes the system toward the cubic structure ($Fm\bar{3}m$; Figure 2c). The structural strain relaxation from $R3m$ to $Fm\bar{3}m$ upon codoping in GeTe provides higher symmetry to the system and thereby increases the electronic band valley degeneracy, which is indeed necessary for increasing the Seebeck coefficient (discussed in a later section).

In order to further understand the influence of the individual dopants (Bi and Sb) on GeTe structure, controlled samples of $Ge_{1-x}Sb_xTe$ (x = 0–0.15) and $Ge_{1-x}Bi_xTe$ (x = 0–0.15) were separately synthesized and PXRD were measured (Figures S1 and S2, Supporting Information, SI). Addition of either Bi or Sb in GeTe does not show the presence of any second phases and the obtained PXRD patterns were indexed into a rhombohedral structure, $R3m$, at room temperature. The similar trends of peak shift toward lower 2θ angle side and convergence of $R3m$ double peaks were observed for an

DOI: 10.1021/acs.chemmater.7b04023
Chem. Mater. 2017, 29, 10426–10435

individual doping of Bi and Sb in GeTe. The calculated lattice parameters for the composition of $Ge_{0.95}Bi_{0.05}Te$ and $Ge_{0.95}Sb_{0.05}Te$ are to be $a = b = 4.1949(6)$ Å and $c = 10.6101(1)$ Å and $a = b = 4.1862$ (6) Å and $c = 10.5701$ (1) Å, respectively. This indicates that Bi doping preferably elongates a and b axes faster than shortening the c axis of GeTe, whereas Sb doping behaves oppositely. This may be due to the slightly larger atomic radius of Bi compared to Sb. Typically, Bi doping promotes $R3m \rightarrow Fm\bar{3}m$ transition slightly faster than Sb doping in GeTe. In order to explore the rhombohedral to cubic phase transition temperatures, DSC measurements were carried out for Bi-, Sb-, and Bi−Sb codoped GeTe samples (Figure S3, SI). Pristine GeTe exhibits a structural transition at ∼700 K, whereas the transition temperature reduces to 656, 634, and 597 K for $Ge_{0.95}Bi_{0.05}Te$, $Ge_{0.90}Sb_{0.10}Te$, and $Ge_{0.85}Bi_{0.05}Sb_{0.10}Te$, respectively. This suggests that codoping of Sb and Bi in GeTe reduces the phase transition temperatures remarkably and increases the cubic nature of the sample.

Transmission electron microscopy (TEM) was carried out to probe nanoscale architectures of Sb and Bi codoped samples. Figure 3a presents the low magnification bright field TEM image of $Ge_{0.85}Bi_{0.05}Sb_{0.10}Te$ sample and the corresponding selected area electron diffraction (SAED) pattern along the zone axis of ⟨1−10⟩ is illustrated in Figure 3b. The SAED pattern could be clearly indexed with the rhombohedral phase ($R3m$). While Figure 3c represents a micrograph of the other area in the sample and its SAED pattern along the zone of axis of the ⟨001⟩ direction is shown in Figure 3d, which could be indexed with a cubic (Fm-$3m$) structure. Thus, upon Sb and Bi codoping, the regions of rhombohedral, $R3m$, and/or the cubic, Fm-$3m$, were randomly distributed in the matrix of GeTe, having good agreement with PXRD data where the presence of both the phases was clearly seen by merging of typical rhombohedral double peaks. Further, Figure 3d illustrates the presence of small nanoprecipitates with a size of ∼15−50 nm embedded in the matrix of GeTe. The inset, Figure 3e, shows the high magnification image of Figure 3d, which emphasizes that observed nanoprecipitates are endotaxial with the matrix of GeTe. Figure 3f shows the high resolution TEM (HRTEM) micrograph of $Ge_{0.85}Bi_{0.05}Sb_{0.10}Te$ with clear interplanar spacing, d, of ∼3.4 Å, which indicates a rhombohedral GeTe matrix, whereas nanoprecipitates have a lattice spacing of ∼3.7 Å for the corresponding (101) plane of Bi. Moreover, the average size and size distribution of the nanoparticles embedded in the $Ge_{0.85}Bi_{0.05}Sb_{0.10}Te$ sample are shown in the SI, Figure S4. The particle size ranges from 15 to 50 nm (see Figure S4a−c, SI), which in fact scatter midwavelength heat carrying phonons significantly, and thereby reduces lattice thermal conductivity. The density of the particles and average size are calculated to be 120 particles/μm^2 and 33 nm, respectively.

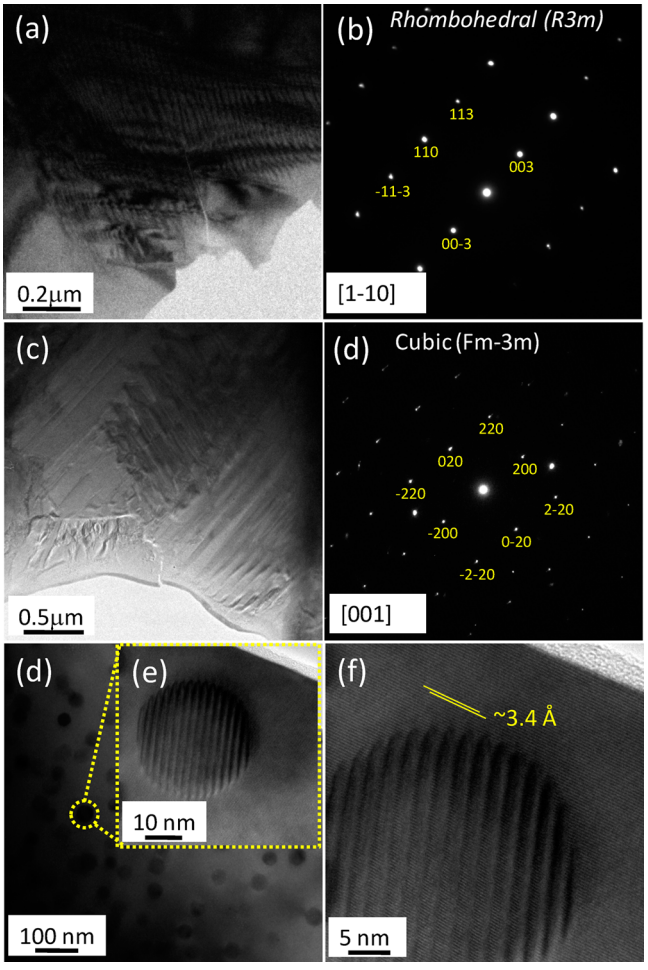

Figure 3. TEM micrographs of $Ge_{0.85}Bi_{0.05}Sb_{0.10}Te$. Panels a and c are the low magnification bright field micrographs, and panels b and d are their corresponding SAED patterns, respectively. Panels e and f are the HRTEM micrographs of the same sample.

The optical band gap of $Ge_{1-x-y}Bi_xSb_yTe$ ($x = 0.02$, 0.05; $y = 0.05$, 0.1) samples were measured by the FT-IR diffuse reflectance spectroscopy (see Figure 2d). Pure GeTe possesses the band gap value of ∼0.21 eV, which agrees with previous reports.[21,27,28] When concentration of Bi and Sb increases in GeTe, the energy band gap reduces from ∼0.21 eV (for GeTe) to ∼0.08 eV ($Ge_{0.85}Bi_{0.05}Sb_{0.10}Te$) due to the formation of donor defect states below the conduction band. In GeTe, the valence band is formed by the Te orbital, while Ge constitutes the conduction band due to the deferences in electronegativity, χ, of Ge ($\chi_{Ge} = 2.01$, in Pauling electronegative scale) and Te ($\chi_{Te} = 2.10$). Aliovalent dopants of Bi and Sb form the donor/impurity states just below the conduction band, because of slightly higher values of electronegativity, χ_{Bi} (2.02) and χ_{Sb} (2.05), compared to that of Ge, which reduces the band gap. The decrease in band gap upon an individual doping of Bi/Sb and codoping of Bi−Sb in GeTe is extensively studied using electronic structure calculations by DFT (see a latter section).

With the understanding of structure, nanostructure, and band gap, we have measured the thermoelectric properties of $Ge_{1-x-y}Bi_xSb_yTe$ ($x = 0.02$, 0.05; $y = 0.05$, 0.1) samples in the temperature range of 300−800 K (Figure 4). Figure 4a shows the temperature dependent electrical conductivity, σ, of $Ge_{1-x-y}Bi_xSb_yTe$, where the σ value of all of the samples decreases with increasing temperature, indicating the typical characteristics of degenerate semiconductor. Typically, pristine GeTe has a σ of ∼8067 S/cm at 300 K, which slowly falls to ∼2095 S/cm at 725 K. Doping of either an individual Bi/Sb or codoping of Sb and Bi in GeTe further reduces the σ. In particular, pure GeTe has a σ of ∼8067 S/cm at 300 K, which drastically reduces to ∼817 S/cm at 300 K for $Ge_{0.85}Bi_{0.05}Sb_{0.10}Te$. This huge reduction in σ is mainly due to the donor dopant nature of Bi^{3+} and Sb^{3+} at the Ge^{2+} site in GeTe and an effective suppression of intrinsic Ge vacancies. Interestingly, addition of Bi and Sb decreases the structural transition temperature of GeTe, which could be clearly seen in

DOI: 10.1021/acs.chemmater.7b04023
Chem. Mater. 2017, 29, 10426−10435

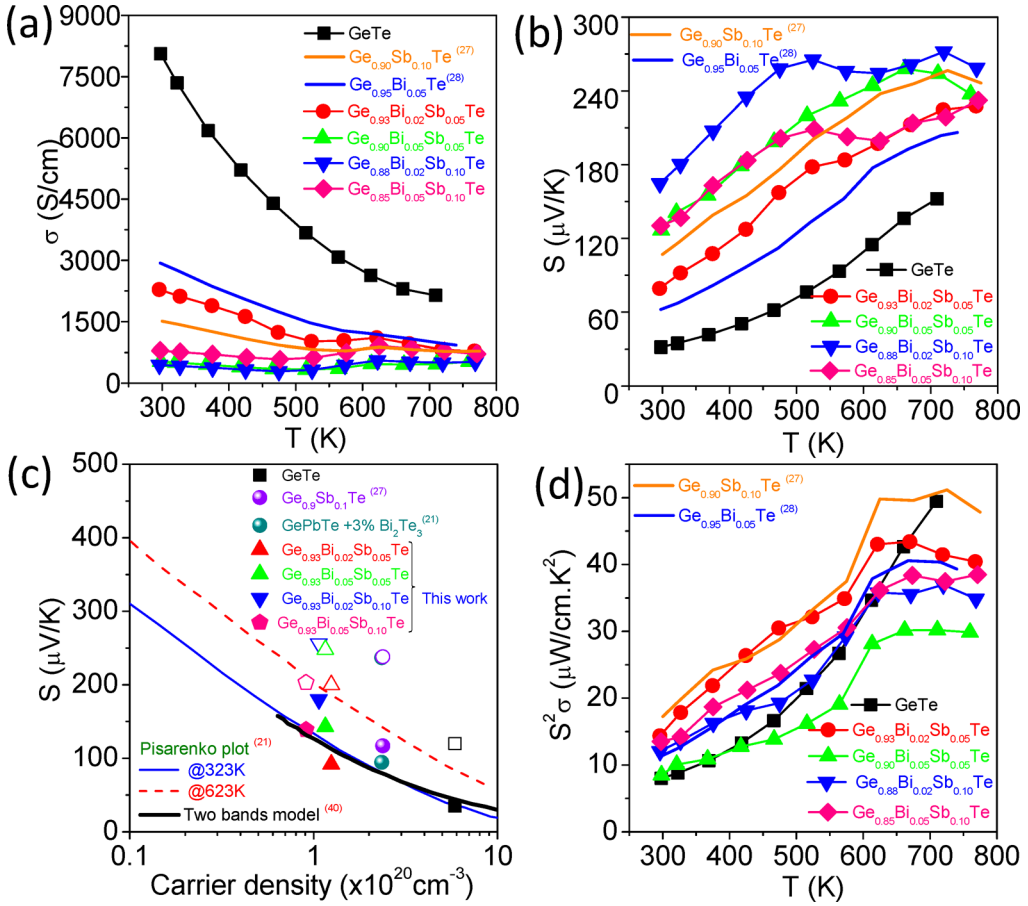

Figure 4. Temperature dependent (a) electrical conductivity and (b) Seebeck coefficient of $Ge_{1-x-y}Bi_xSb_yTe$; (c) Pisarenko plot (S vs n) at 323 (blue solid line) and 623 K (red dashed line) and two bands model (black solid line). Solid and open symbols denote the S vs n data at 323 and 623 K, respectively. (d) Power factor of $Ge_{1-x-y}Bi_xSb_yTe$ samples.

Figure 4a. For example, σ of all the doped samples decreases with increasing temperature up to 525 K, and then σ slightly starts increasing until 625 K and above which it falls down again. This is a clear signature of second order structural transition ($R3m \rightarrow Fm\text{-}3m$) of GeTe. Hall measurements were carried out for all samples of $Ge_{1-x-y}Bi_xSb_yTe$ to understand the large suppression of p-type carrier concentration (n_p) upon Bi and Sb codoping. Typically, pure GeTe has a n_p value of $\sim 6 \times 10^{20}$ cm^{-3}, which gradually decreases to $\sim 1.25 \times 10^{20}$, $\sim 1.16 \times 10^{20}$, $\sim 1.07 \times 10^{20}$, and $\sim 9.1 \times 10^{19}$ cm^{-3} for the compositions of $Ge_{0.93}Bi_{0.02}Sb_{0.05}Te$, $Ge_{0.90}Bi_{0.05}Sb_{0.05}Te$, $Ge_{0.88}Bi_{0.02}Sb_{0.10}Te$, and $Ge_{0.85}Bi_{0.05}Sb_{0.10}Te$, respectively. To explore the scattering mechanism, the carrier mobility, μ_H, of $Ge_{1-x-y}Bi_xSb_yTe$ samples at room temperature is also estimated. Pristine GeTe possesses a μ_H of ~ 83 $cm^2/(V\ s)$ at 300 K which rises to ~ 114 $cm^2/(V\ s)$ for $Ge_{0.93}Bi_{0.02}Sb_{0.05}Te$ due to a significant suppression of Ge vacancies and carrier concentration, n_p. The μ_H value further reduces to ~ 29, 27, and 56 $cm^2/(V\ s)$ for the compositions of $Ge_{0.90}Bi_{0.05}Sb_{0.05}Te$, $Ge_{0.88}Bi_{0.02}Sb_{0.10}Te$, and $Ge_{0.85}Bi_{0.05}Sb_{0.10}Te$ due to an enhanced point defect carrier scattering.

Figure 4b presents the temperature dependent Seebeck coefficient, S, of $Ge_{1-x-y}Bi_xSb_yTe$ ($x = 0.02, 0.05$; $y = 0.05, 0.1$). The measured S of all of the samples shows the positive values and the S increases with the increase in temperature. In this context, the S value of undoped GeTe is ~ 32 $\mu V/K$ at 300 K, which monotonically increases up to ~ 155 $\mu V/K$ at 725 K. When the doping concentration of Sb and Bi increases in GeTe, the S values rapidly increases to ~ 165 $\mu V/K$ at 300 K and further reaches a maximum value of ~ 272 $\mu V/K$ at 720 K for $Ge_{0.88}Bi_{0.02}Sb_{1.0}Te$. Moreover, the S value of $Ge_{0.88}Bi_{0.02}Sb_{1.0}Te$ is to be ~ 266 $\mu V/K$ at 525 K, and then it decreases to ~ 255 $\mu V/K$ at 625 K, and with increasing the temperature, the S value further increases until 720 K. This trend is a clear indication of $R3m \rightarrow Fm\text{-}3m$ transition and agrees well with σ vs T data.

In order to understand the enhancement of the Seebeck coefficient in Bi and Sb codoped GeTe, the carrier density dependent Seebeck coefficients of $Ge_{1-x-y}Bi_xSb_yTe$ were plotted and compared with the previously reported Pisarenko plot of GeTe at 323 and 623 K, which was calculated based on single parabolic band model (see Figure 4c).[21] Additionally, we have also compared the experimental Seebeck data with the Pisarenko plot of GeTe, which was calculated considering the two band model previously.[40] In pristine GeTe, the experimental S value follows the Pisarenko line at 323 K, while it slightly deviates when the temperature reaches to 623 K, suggesting that the second valence band (Σ band) takes over the conduction of carriers from principal valence band (L band) at high T. With codoping of Sb and Bi in GeTe, the S values deviate and fall above the Pisarenko lines calculated using both the single parabolic band[21] and two band model.[40] Thus, codoping of Sb and Bi in GeTe alters the electronic structure of GeTe and promotes the conduction of the heavy hole valence band over light hole valence band.

To further clarify the enhancement of S, we have calculated the effective mass (m^*) of the carriers in $Ge_{1-x-y}Bi_xSb_yTe$ using

DOI: 10.1021/acs.chemmater.7b04023
Chem. Mater. 2017, 29, 10426−10435

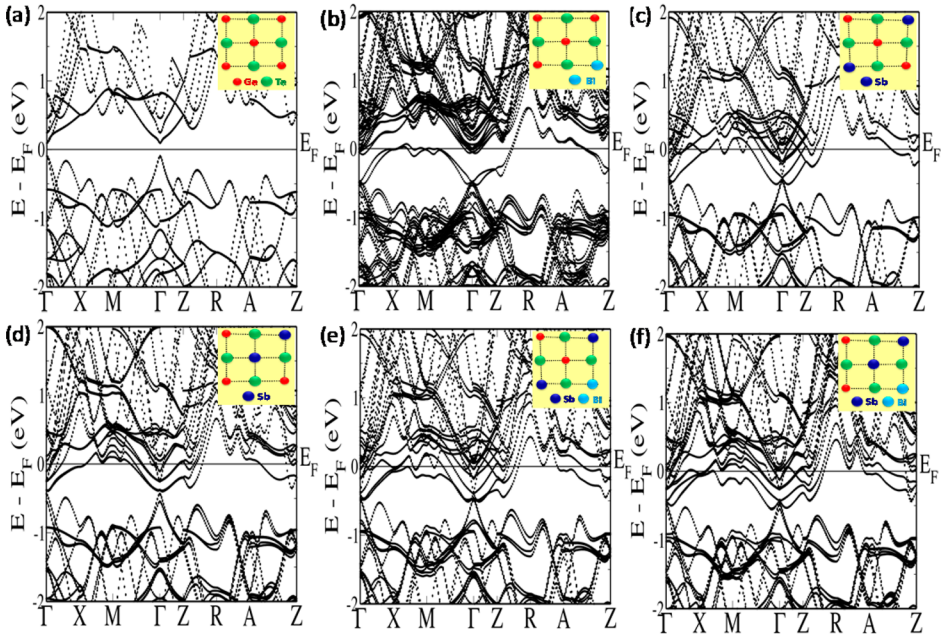

Figure 5. Electronic structures of (a) $Ge_{16}Te_{16}$, (b) $Ge_{15}BiTe_{16}$, (c) $Ge_{14}Sb_2Te_{16}$ (Sb atoms far from one another), (d) $Ge_{14}Sb_2Te_{16}$ (Sb atoms close to one another), and (e and f) $Ge_{13}BiSb_2Te_{16}$ with Sb atoms far (e) and close to each other (f), respectively. The band gap appears at the Γ point and heavy-hole band at Z + δ in the $\sqrt{2} \times \sqrt{2} \times 2$ tetragonal supercell. The VBM and CBM occurring at the L point in the rocksalt cell of GeTe fold onto the Γ point, and the heavy-hole valence band appearing along Σ folds onto Z + δ along Z → R direction in the case of the present 32 atom $\sqrt{2} \times \sqrt{2} \times 2$ tetragonal supercell.

the experimental S and carrier density (n) data measured at 300 K, by the following expressions (eqs 1−3):[12,21,27]

$$m^* = \frac{h^2}{2k_B T}\left[\frac{n}{4\pi F_{1/2}(\eta)}\right]^{2/3} \quad (1)$$

$$S = \pm\frac{k_B}{e}\left(\frac{(r+3/2)F_{r+3/2}(\eta)}{(r+3/2)F_{r+1/2}(\eta)} - \eta\right) \quad (2)$$

$$F_n(\eta) = \int_0^\infty \frac{x^n}{1+e^{x-\eta}}\,dx \quad (3)$$

where η, $F_n(\eta)$, k_B, e, h, and r stand for reduced Fermi energy, nth order Fermi integral, the Boltzmann constant, electron charge, Planck constant, and scattering factor, respectively. The reduced Fermi energy was calculated by fitting the corresponding experimental Seebeck data. The m^* values were calculated based on a single parabolic band, where acoustic phonon scatterings are only considered with $r = -1/2$ for simplicity.[12,21,27] The calculated m^* value of pristine GeTe is 1.10 m_0, which increases to 2.44 m_0 for the composition of $Ge_{0.88}Bi_{0.02}Sb_{0.10}Te$ and thereby indicates that enhanced valence band degeneracy increases the Seebeck values in $Ge_{1-x-y}Bi_xSb_yTe$.

Moreover, to understand the reason behind the observed enhancement in S values of the $Ge_{1-x-y}Bi_xSb_yTe$ system, we have used DFT to determine the electronic structure of pristine, Bi-doped, Sb-doped, and Bi−Sb codoped GeTe (see Figure 5). The electronic structure of the cubic phase of GeTe resembles that of PbTe, with four ⟨111⟩ extrema in the band energies around the L point and 12 ⟨110⟩ extrema around the Σ point. When GeTe experiences a cubic-to-rhombohedral phase transition around 700 K, the symmetry of the system gets lowered. However, since this distortion is weak and the rhombohedral phase is nearly face-centered cubic and Bi and Sb codoping increases the cubic character of GeTe, the electronic structure of GeTe can be analyzed in terms of its cubic structure (as the splitting of degeneracy of bands is negligible), which was also assumed in earlier electronic structure calculations.[21] In the current calculations, the principal valence band (light hole) maximum (VBM) and conduction band minimum (CBM) occur at the Γ point due to folding of the L point onto Γ. Second, the heavy hole band which normally appears at a point along Σ occurs at Z + δ along the Z → R direction in the Brillouin zone of the 32 atom ($\sqrt{2} \times \sqrt{2} \times 2$) tetragonal supercell. In the electronic structure of $Ge_{16}Te_{16}$ (Figure 5a), we see a band gap of 0.192 eV at the Γ point agreeing well with the present experimental results and earlier theoretical calculations.[21,27,28,39] Our estimate of the energy difference ($\Delta E_{\Gamma\text{-}ZR}$) between the light and heavy hole valence bands of undoped cubic GeTe is 0.202 eV, which is consistent with the literature.[21,41] To mimic the experimental composition of the codoped sample, one Bi atom and two Sb atoms were substituted for Ge atoms in GeTe.

For 6.25 mol % substitution of Bi at Ge in GeTe, a new impurity/donor band arises from Bi states, which reduces the principal band gap of GeTe (Figure 5b). The difference ($\Delta E_{\Gamma\text{-}ZR}$) in Bi doped GeTe is 0.201 eV, which is close to that of pristine GeTe. To simulate 12.5 mol % of Sb doping, two Sb atoms were substituted for two Ge atoms in GeTe. When the substituted Sb atoms are far from one another (inset of Figure 5c), the impurity induced bands are split off from the lower conduction band closing the principal band gap (Figure 5c), while $\Delta E_{\Gamma\text{-}ZR}$ (~0.203 eV) remains unchanged from that of pristine GeTe. However, when Sb atoms are close to one another (inset of Figure 5d) a small band gap (0.049 eV) opens up (Figure 5d). In this case, the $\Delta E_{\Gamma\text{-}ZR}$ reduces to 0.161 eV. We note that the latter configuration is lower in energy than the former, consistent with the idea that opening of a gap enhances

DOI: 10.1021/acs.chemmater.7b04023
Chem. Mater. 2017, 29, 10426−10435

the stability. Similar features are retained in Bi and Sb codoped samples as seen in Figure 5e,f. Upon codoping of Bi and Sb in GeTe, the energy separation between two valence bands, $\Delta E_{\Gamma\text{-}ZR}$, further decreases to 0.151 eV when the Sb atoms are far from one another (Figure 5e). However, when Sb atoms are close to one another, a small principal band gap (0.026 eV) exists (Figure 5f), and the $\Delta E_{\Gamma\text{-}ZR}$ is estimated to be 0.176 eV. It is interesting that the configuration of the codoped system with Sb atoms far from one another is lower in energy, in contrast to just the Sb doped system. Thus, our calculations indicate a significant interaction between substituted Bi- and Sb- and that Bi- and Sb-codoping in GeTe enhances the valence band convergence, which increases the Seebeck coefficient.

We now examine the density of states (DOS) of pristine GeTe and Bi-, Sb-, and codoped (Bi and Sb) GeTe (shown in Figure 6). When intrinsic Ge vacancies are not considered, the

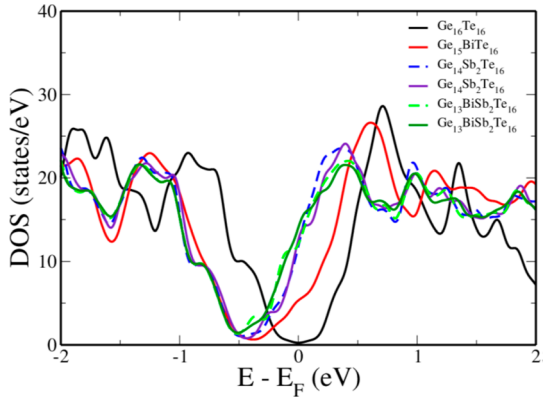

Figure 6. Density of electronic states of pure GeTe and Bi-, Sb-, and codoped (Sb and Bi) GeTe samples. Dashed lines represent the case where Sb atoms are far from each other.

DOS plot reveals that the Fermi level (E_F) is well within the conduction band of the doped samples (Figure 6). Thus, from the DFT calculations, it is clear that doping of Bi/Sb and Bi−Sb form donor states just below the conduction band of GeTe. In addition, it promotes the valence band convergence causing an increased asymmetry in the density of electronic states near the E_F.

The power factor ($S^2\sigma$) of $Ge_{1\text{-}x\text{-}y}Bi_xSb_yTe$ systems as a function of temperature is shown in Figure 4d. In pristine GeTe, $S^2\sigma$ has the value of ~8.4 μW/cmK^2 at 300 K, which reached the maximum value of ~49.4 μW/cmK^2 at 700 K. Typically, the $Ge_{0.93}Bi_{0.02}Sb_{0.05}Te$ sample exhibits the $S^2\sigma$ value of ~14.5 μW/cmK^2 at 300 K, which increases to ~43.2 μW/cmK^2 at 625 K. Above 625 K, $S^2\sigma$ remains almost flat with increasing the temperature for all codoped samples.

The temperature dependences of total (κ_{total}), electronic (κ_{el}), and lattice thermal conductivity (κ_{lat}) of $Ge_{1\text{-}x\text{-}y}Bi_xSb_yTe$ are shown in Figure 7a−c. The κ_{total} of all samples decreases with increasing temperature in the measured temperature range of 300−800 K. Typically, κ_{total} of GeTe is ~8.3 W/mK at 300 K, which decreases to ~3.4 W/mK at 625 K and then it starts to increase slightly due to $R3m \rightarrow Fm\text{-}3m$ structural transition. Codoping of Bi and Sb in GeTe rapidly reduces the κ_{total}. In particular, the κ_{total} value decreases from ~8.3 to ~0.95 W/mK at 300 K for the composition of $Ge_{0.85}Bi_{0.05}Sb_{0.10}Te$, which is in fact about ~89% reduction as compared to pristine GeTe. In addition, codoping of Bi and Sb decreases the structural phase

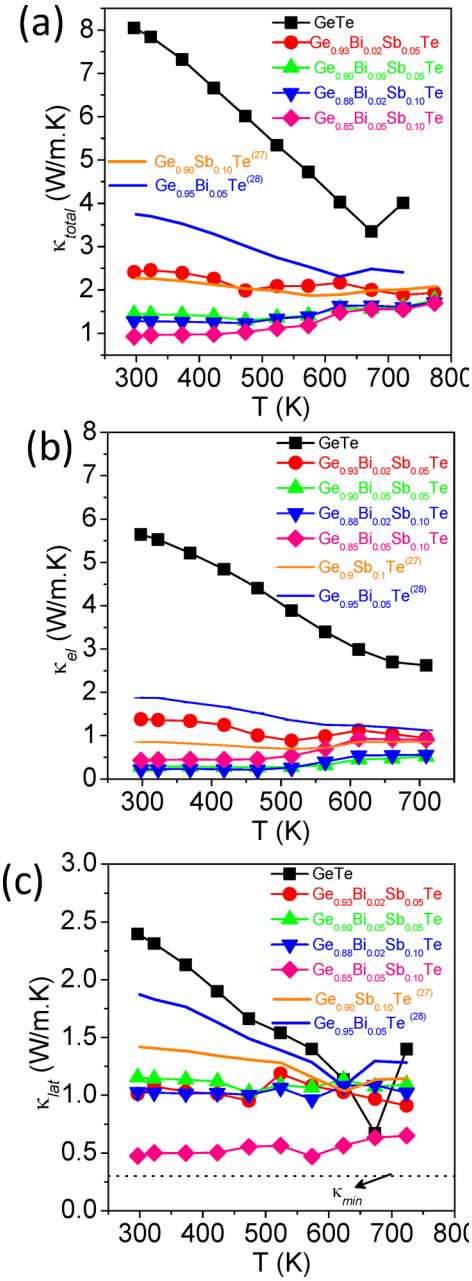

Figure 7. Temperature dependence of (a) total thermal conductivity (κ_{total}), (b) electronic thermal conductivity (κ_{el}), and (c) lattice thermal conductivity (κ_{lat}).

transition temperature from 675 to 550 K which is clearly seen in the temperature dependent κ_{total} data.

The calculated carrier contribution to thermal conductivity, ($\kappa_{el} = L\sigma T$) as a function of temperature is shown in Figure 7b. Here, the temperature dependent Lorentz number, L, was calculated from the fitting of temperature dependent experimental Seebeck data using simple parabolic band model, from the following equation:[12,21,27]

$$L = \left(\frac{k_B}{e}\right)^2 \frac{3F_0(\eta)F_2(\eta) - 4F_1(\eta)^2}{F_0(\eta)^2} \quad (4)$$

κ_{el} value of all of the $Ge_{1\text{-}x\text{-}y}Bi_xSb_yTe$ samples are decreased with increasing temperature and codoping of Bi and Sb in GeTe further reduces the κ_{el} compared to that of pristine GeTe. In

DOI: 10.1021/acs.chemmater.7b04023
Chem. Mater. 2017, 29, 10426−10435

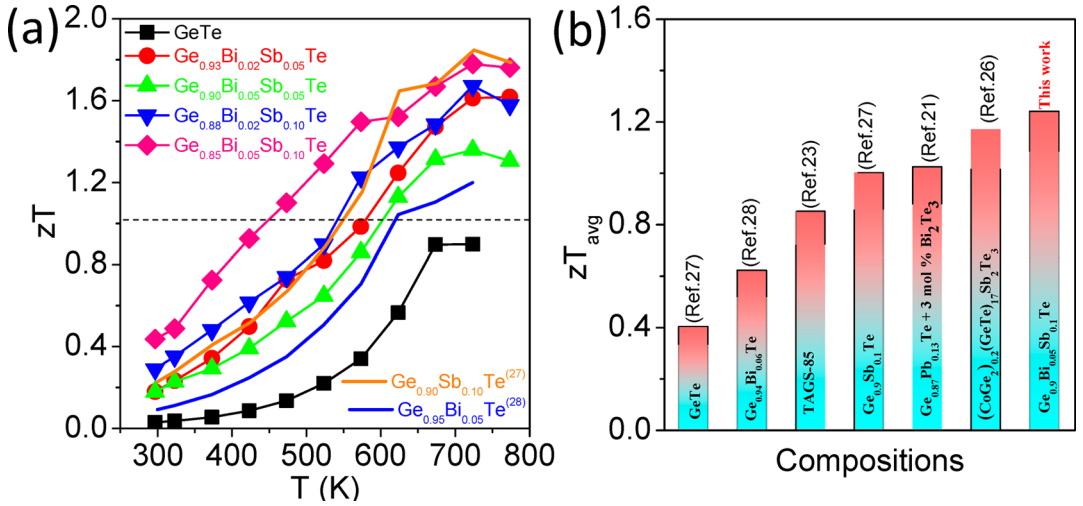

Figure 8. (a) Temperature dependence dimensionless thermoelectric figure of merit (zT) of $Ge_{1-x-y}Bi_xSb_yTe$ system and (b) comparison of average thermoelectric figure of merit, zT_{avg} of selected GeTe based materials[21,23,26−28] with the present $Ge_{0.85}Sb_{0.10}Bi_{0.05}Te$ sample.

particular, the κ_{el} of GeTe is ∼5.6 W/mK at 300 K, which has dominant contribution to κ_{total}. Co-doping strongly suppresses the κ_{el} to ∼0.45 W/mK at 300 K for $Ge_{0.85}Bi_{0.05}Sb_{0.10}Te$ due to the donor nature of Sb and Bi. The reduction in κ_{el} is about ∼92% as compared to that of pristine GeTe. Figure S5 (see the Supporting Information) shows the temperature dependence of the estimated Lorentz number, thermal diffusivity, and specific heat capacity of $Ge_{1-x-y}Bi_xSb_yTe$ samples.

The lattice contribution to thermal conductivity (κ_{lat}) of $Ge_{1-x-y}Bi_xSb_yTe$ samples is calculated by subtracting the κ_{el} from κ_{total}, and the values of κ_{lat} are presented in Figure 7c. The κ_{lat} of all samples decreases with increasing temperature. Addition of Sb and Bi decreases κ_{lat} significantly. GeTe has a κ_{lat} value of ∼2.4 W/mK at 300 K, which encounters significant reduction to ∼0.5 W/mK for $Ge_{0.85}Bi_{0.05}Sb_{0.10}Te$. Interestingly, Sb and Bi codoped GeTe demonstrate larger reduction of κ_{lat} compared to that of the controlled single doped (Sb/Bi) GeTe samples (refer to Figure 7c). This significant reduction is attributed to synergistic phonon scattering by the observed small sized Bi rich nanoprecipitates and atomic-scale point defects due to mass-fluctuations created by Sb in place of Ge in GeTe. Bi forms small nanoprecipitates in the GeTe matrix due to large size mismatch, while Sb prefers to form solid solution in GeTe, and thus, Sb and Bi have complementary roles in reduction of κ_{latt} in GeTe.

The temperature dependence dimensionless figure of merit (zT) and zT_{avg} of $Ge_{1-x-y}Bi_xSb_yTe$ samples are presented in Figure 8. From Figure 8a, it is clearly seen that the zT of all samples increases with temperature and particularly, pristine GeTe has a zT of ∼0.03 at 300 K, which rises to ∼0.9 at 675 K. Upon codoping of Sb and Bi, the zT enhances substantially, and the maximum zT of ∼1.8 at 725 K was achieved for the composition of $Ge_{0.85}Bi_{0.05}Sb_{0.10}Te$. The large enhancement of zT in $Ge_{1-x-y}Bi_xSb_yTe$ was obtained due the collective reasons of (i) suppression of *p*-type carrier concentration along with intrinsic Ge vacancies, (ii) significant enhancement in the Seebeck coefficient driven by valence band convergence and cubic structure induced enhanced valley degeneracy, and (iii) large reduction of lattice thermal conductivity due to synergistic phonon scattering by solid solution point defects and nanoprecipitates. Interestingly, $Ge_{0.85}Bi_{0.05}Sb_{0.10}Te$ possesses a maximum zT_{avg} value of ∼1.24 in the temperature range of 300−725 K (see Figure 8b), which is the notably highest among the selected GeTe based materials.[21,23,26−28]

CONCLUSIONS

Interplay between complementary roles of Sb and Bi substitution in GeTe is shown to result in high thermoelectric figure of merit of ∼1.8 at 725 K with zT_{avg} of 1.24 in $Ge_{1-x-y}Bi_xSb_yTe$ samples. High thermoelectric performance is achieved by the simultaneous enhancement of the Seebeck coefficient and lowering the lattice thermal conductivity. Sb and Bi codoping enhances the stability of the cubic structure in GeTe, thereby increasing the valence band degeneracy, which is beneficial for enhancement of the Seebeck coefficient. Moreover, Sb substitution reduces the gap between light and heavy hole valence bands of GeTe, which further improves the Seebeck coefficient through valence band convergence. In addition, Bi forms nanoprecipitates in the GeTe matrix which scatter phonons effectively and Sb creates solid solution point defects in GeTe, which all-together reduces the lattice thermal conductivity noticeably to ∼0.5 W/mK in $Ge_{1-x-y}Bi_xSb_yTe$. Thus, our work should motivate chemists and materials scientists to investigate the effect of complementary codoping in the thermoelectric system rather than conventional single doping.

ASSOCIATED CONTENT

Supporting Information

The Supporting Information is available free of charge on the ACS Publications website at DOI: 10.1021/acs.chemmater.7b04023.

Figures S1−S6. Additional PXRD, DSC, TEM, size distribution data, temperature dependent on Lorentz number, thermal diffusivity, specific heat, and reproducibility of zT. (PDF)

AUTHOR INFORMATION

Corresponding Author

*E-mail: kanishka@jncasr.ac.in.

ORCID

Umesh V. Waghmare: 0000-0002-9378-155X

Kanishka Biswas: 0000-0001-9119-2455

DOI: 10.1021/acs.chemmater.7b04023
Chem. Mater. 2017, 29, 10426−10435

Notes

The authors declare no competing financial interest.

■ ACKNOWLEDGMENTS

K.B. acknowledges funding support from Nano mission, DST (SR/NM/TP-25/2016) and SERB (EMR/2016/000651). K.B. also acknowledges Sheik Saqr Laborator, JNCASR. S.P. thanks TRC-project (TRC-JNC/KB/4396) in JNCASR. U.V.W. acknowledges funding from IKST and a J C Bose National Fellowship of the DST. We thank Prof. N. Ravishankar (IISc) for fruitful discussion on TEM analysis.

■ REFERENCES

(1) Sootsman, J.; Chung, D. Y.; Kanatzidis, M. G. New and Old Concepts in Thermoelectric Materials. *Angew. Chem., Int. Ed.* **2009**, *48*, 8616−8639.

(2) Zhao, L. D.; Dravid, V. P.; Kanatzidis, M. G. The panoscopic approach to high performance thermoelectrics. *Energy Environ. Sci.* **2014**, *7*, 251−268.

(3) Tan, G.; Zhao, L.-D.; Kanatzidis, M. G. Rationally Designing High-Performance Bulk Thermoelectric Materials. *Chem. Rev.* **2016**, *116*, 12123−12149.

(4) Kim, H. S.; Liu, W.; Chen, G.; Chu, C.-W.; Ren, Z. Relationship between thermoelectric figure of merit and energy conversion efficiency. *Proc. Natl. Acad. Sci. U. S. A.* **2015**, *112*, 8205−82101.

(5) Faleev, S. V.; Leonard, F. Theory of enhancement of thermoelectric properties of materials with nanoinclusions. *Phys. Rev. B: Condens. Matter Mater. Phys.* **2008**, *77*, 214304.

(6) Heremans, J. P.; Jovovic, V.; Toberer, E. S.; Saramat, A.; Kurosaki, K.; Charoenphakdee, A.; Yamanaka, S.; Snyder, G. J. Enhancement of Thermoelectric Efficiency in PbTe by Distortion of the Electronic Density of States. *Science* **2008**, *321*, 554−557.

(7) Pei, Y.; Shi, X.; LaLonde, A.; Wang, H.; Chen, L.; Snyder, G. J. Convergence of electronic bands for high performance bulk thermoelectrics. *Nature* **2011**, *473*, 66−69.

(8) Liu, W.; Tan, X.; Yin, K.; Liu, H.; Tang, X.; Shi, J.; Zhang, Q.; Uher, C. Convergence of Conduction Bands as a Means of Enhancing Thermoelectric Performance of n-Type $Mg_2Si_{1-x}Sn_x$ Solid Solutions. *Phys. Rev. Lett.* **2012**, *108*, 166601.

(9) Hicks, L. D.; Dresselhaus, M. S. Effect of quantum-well structures on the thermoelectric Figure of merit. *Phys. Rev. B: Condens. Matter Mater. Phys.* **1993**, *47*, 12727−12731.

(10) Biswas, K.; He, J.; Zhang, Q.; Wang, G.; Uher, C.; Dravid, V. P.; Kanatzidis, M. G. Strained endotaxial nanostructures with high thermoelectric figure of merit. *Nat. Chem.* **2011**, *3*, 160−166.

(11) Biswas, K.; He, J.; Blum, I. D.; Wu, C. I.; Hogan, T. P.; Seidman, D. N.; Dravid, V. P.; Kanatzidis, M. G. High-performance bulk thermoelectrics with all-scale hierarchical architectures. *Nature* **2012**, *489*, 414−418.

(12) Morelli, D. T.; Jovovic, V.; Heremans, J. P. Intrinsically Minimal Thermal Conductivity in Cubic I-V-VI2 Semiconductors. *Phys. Rev. Lett.* **2008**, *101*, 035901.

(13) Guin, S. N.; Chatterjee, A.; Negi, D. S.; Datta, R.; Biswas, K. High thermoelectric performance in tellurium free p-type $AgSbSe_2$. *Energy Environ. Sci.* **2013**, *6*, 2603−2608.

(14) Skrabek, E. A.; Trimmer, D. S. *Thermoelectrics Handbook*; Rowe, D. M., Ed.; CRC: Boca Raton, FL, 1995; Chapter 22.

(15) Lewis, J. E. The Defect Structure of Non Stoichiometric Germanium Telluride from Magnetic Susceptibility Measurements. *Phys. Status Solidi B* **1970**, *38*, 131−140.

(16) Damon, D. H.; Lubell, M. S.; Mazelsky, R. Nature of the defects in germanium telluride. *J. Phys. Chem. Solids* **1967**, *28*, 520−522.

(17) Banik, A.; Shenoy, U. S.; Saha, S.; Waghmare, U. V.; Biswas, K. High power factor and enhanced thermoelectric performance of SnTe-$AgInTe_2$: Synergistic effect of resonance level and valence band convergence. *J. Am. Chem. Soc.* **2016**, *138* (39), 13068−13075.

(18) Banik, A.; Vishal, B.; Perumal, S.; Datta, R.; Biswas, K. The origin of low thermal conductivity in $Sn_{1-x}Sb_xTe$: phonon scattering *via* layered intergrowth nanostructures. *Energy Environ. Sci.* **2016**, *9*, 2011−2019.

(19) Perumal, S.; Roychowdhury, S.; Biswas, K. High performance thermoelectric materials and devices based on GeTe. *J. Mater. Chem. C* **2016**, *4*, 7520−7536.

(20) Gelbstein, Y.; Davidow, J. Highly efficient functional $Ge_xPb_{1-x}Te$ based thermoelectric alloys. *Phys. Chem. Chem. Phys.* **2014**, *16*, 20120−20126.

(21) Wu, D.; Zhao, L. D.; Hao, S.; Jiang, Q.; Zheng, F.; Doak, J. W.; Wu, H.; Chi, H.; Gelbstein, Y.; Uher, C.; Wolverton, C.; Kanatzidis, M. G.; He, J. Origin of the high performance in GeTe-based thermoelectric materials upon Bi_2Te_3 doping. *J. Am. Chem. Soc.* **2014**, *136*, 11412−11419.

(22) Davidow, J.; Gelbstein, Y. A Comparison Between the Mechanical and Thermoelectric Properties of Three Highly Efficient *p*-Type GeTe-Rich Compositions: TAGS-80, TAGS-85, and 3% Bi_2Te_3-Doped $Ge_{0.87}Pb_{0.13}Te$. *J. Electron. Mater.* **2013**, *42*, 1542−1549.

(23) Salvador, J. R.; Yang, J.; Shi, X.; Wang, H.; Wereszczak, A. A. Transport and mechanical property evaluation of $(AgSbTe)_{1-x}(GeTe)_x$ (x = 0.80, 0.82, 0.85, 0.87, 0.90). *J. Solid State Chem.* **2009**, *182*, 2088−2095.

(24) Chen, Y.; Jaworski, C. M.; Gao, Y. B.; Wang, H.; Zhu, T. J.; Snyder, G. J.; Heremans, J. P.; Zhao, X. B. Transport properties and valence band feature of high-performance $(GeTe)_{85}(AgSbTe_2)_{15}$ thermoelectric materials. *New J. Phys.* **2014**, *16*, 013057.

(25) Samanta, M.; Roychowdhury, S.; Ghatak, J.; Perumal, S.; Biswas, K. Ultrahigh Average Thermoelectric Figure of Merit, Low Lattice Thermal Conductivity and Enhanced Microhardness in Nanostructured $(GeTe)_x$ $(AgSbSe_2)_{100-x}$. *Chem. - Eur. J.* **2017**, *23*, 7438−7443.

(26) Fahrnbauer, F.; Souchay, D.; Wagner, G.; Oeckler, O. High thermoelectric figure of merit values of germanium antimony tellurides with kinetically stable cobalt germanide precipitates. *J. Am. Chem. Soc.* **2015**, *137*, 12633−12638.

(27) Perumal, S.; Roychowdhury, S.; Negi, D. S.; Datta, R.; Biswas, K. High Thermoelectric Performance and Enhanced Mechanical Stability of p-type $Ge_{1-x}Sb_xTe$. *Chem. Mater.* **2015**, *27*, 7171−7178.

(28) Perumal, S.; Roychowdhury, S.; Biswas, K. Reduction of thermal conductivity through nanostructuring enhances the thermoelectric figure of merit in $Ge_{1-x}Bi_xTe$. *Inorg. Chem. Front.* **2016**, *3*, 125−132.

(29) Li, J.; Zhang, X.; Lin, S.; Chen, Z.; Pei, Y. Realizing the high thermoelectric performance of GeTe by Sb-doping and Se-alloying. *Chem. Mater.* **2017**, *29*, 605−611.

(30) Samanta, M.; Biswas, K. Low Thermal Conductivity and High Thermoelectric Performance in $(GeTe)_{1-2x}(GeSe)_x(GeS)_x$: Competition between Solid Solution and Phase Separation. *J. Am. Chem. Soc.* **2017**, *139*, 9382−9391.

(31) Okamoto, H.; Massalski, T. B. *Binary Alloy Phase Diagrams*, 2nd ed.; ASM International: Novelty, OH, 1990.

(32) Cook, B.; Wei, X.; Harringa, J.; Kramer, M. In-situ elevated-temperature TEM study of $(AgSbTe_2)_{15}(GeTe)_{85}$. *J. Mater. Sci.* **2007**, *42*, 7643−7646.

(33) Bauer Pereira, P.; Sergueev, I.; Gorsse, S.; Dadda, J.; Muller, E.; Hermann, R. P. Lattice dynamics and structure of GeTe, SnTe and PbTe. *Phys. Status Solidi B* **2013**, *250*, 1300−1307.

(34) Levin, E. M.; Besser, M. F.; Hanus, R. Electronic and thermal transport in GeTe: A versatile base for thermoelectric materials. *J. Appl. Phys.* **2013**, *114*, 083713.

(35) Perumal, S.; Gorsse, S.; Ail, U.; Prakasam, M.; Chevalier, B.; Umarji, A. M. Thermoelectric properties of chromium disilicide prepared by mechanical alloying. *J. Mater. Sci.* **2013**, *48*, 6018−6024.

(36) Giannozzi, P.; Baroni, S.; Bonini, N.; Calandra, M.; Car, R.; Cavazzoni, C.; Ceresoli, D.; Chiarotti, G. L.; Cococcioni, M.; Dabo, I.; Dal Corso, A.; de Gironcoli, S.; Fabris, S.; Fratesi, G.; Gebauer, R.; Gerstmann, U.; Gougoussis, C.; Kokalj, A.; Lazzeri, M.; Martin-Samos, L.; Marzari, N.; Mauri, F.; Mazzarello, R.; Paolini, S.; Pasquarello, A.; Paulatto, L.; Sbraccia, C.; Scandolo, S.; Sclauzero, G.; Seitsonen, A. P.; Smogunov, A.; Umari, P.; Wentzcovitch, R. M. QUANTUM

DOI: 10.1021/acs.chemmater.7b04023
Chem. Mater. 2017, 29, 10426−10435

ESPRESSO: a modular and open-source software project for quantum simulations of materials. *J. Phys.: Condens. Matter* **2009**, *21*, 395502.
(37) Perdew, J. P.; Burke, K.; Ernzerhof, M. Generalized gradient approximation made simple. *Phys. Rev. Lett.* **1996**, *77*, 3865−3868.
(38) Schlieper, A.; Feutelais, Y.; Fries, S. G.; Legendre, B.; Blachnik, R. Thermodynamic evaluation of the Germanium—Tellurium system. *CALPHAD: Comput. Coupling Phase Diagrams Thermochem.* **1999**, *23*, 1−18.
(39) Hoang, K.; Mahanti, S. D.; Kanatzidis, M. G. Impurity clustering and impurity-induced bands in PbTe-, SnTe-, and GeTe-based bulk thermoelectrics. *Phys. Rev. B: Condens. Matter Mater. Phys.* **2010**, *81*, 115106.
(40) Li, J.; Chen, Z.; Zhang, X.; Sun, Y.; Yang, J.; Pei, Y. Electronic origin of the high thermoelectric performance of GeTe among the p-type group IV monotellurides. *NPG Asia Mater.* **2017**, *9*, e353.
(41) Lewis, J. E. Optical properties and energy gap of GeTe form reflectance studies. *Phys. Status Solidi B* **1973**, *59*, 367−377.

DOI: 10.1021/acs.chemmater.7b04023
Chem. Mater. 2017, 29, 10426−10435